Enhancement of Thermoelectric Efficiency in PbTe by Distortion of the Electronic Density of States

Joseph P. Heremans *et al.*

Science **321**, 554 (2008);
DOI: 10.1126/science.1159725

Science (print ISSN 0036-8075; online ISSN 1095-9203) is published weekly, except the last week in December, by the American Association for the Advancement of Science, 1200 New York Avenue NW, Washington, DC 20005.

were likely initiated by this favorable climate regime.

References and Notes

1. J. C. Zachos, L. D. Stott, K. C. Lohmann, *Paleoceanography* **9**, 353 (1994).
2. J. Veizer *et al.*, *Chem. Geol.* **161**, 59 (1999).
3. G. A. Shields *et al.*, *Geochim. Cosmochim. Acta* **67**, 2005 (2003).
4. J. Veizer, Y. Godderis, L. M. François, *Nature* **408**, 698 (2000).
5. J. Veizer, P. Fritz, B. Jones, *Geochim. Cosmochim. Acta* **50**, 1679 (1986).
6. K. Azmy, J. Veizer, M. G. Bassett, P. Copper, *Geol. Soc. Am. Bull.* **110**, 1499 (1998).
7. J. F. Kasting *et al.*, *Earth Planet. Sci. Lett.* **252**, 82 (2006).
8. R. T. Gregory, H. P. Taylor, *J. Geophys. Res.* **86**, 2737 (1981).
9. K. Muehlenbachs, *Chem. Geol.* **145**, 263 (1998).
10. C. Lécuyer, P. Allemand, *Geochim. Cosmochim. Acta* **63**, 351 (1999).
11. R. T. Gregory, in *Stable Isotope Geochemistry: A Tribute to Samuel Epstein*, H. P. Taylor, J. R. O'Neill, I. R. Kaplan, Eds. (Geochemical Society Special Publication, University Park, PA, 1991), vol. 3, pp. 65–76.
12. J. J. Sepkoski, in *Global Events and Event Stratigraphy in the Phanerozoic: Results of International Interdisciplinary Cooperation in the IGCP Project 216 "Global Biological Events in Earth History,"* O. H. Walliser, Ed. (Springer-Verlag, Berlin, 1996), pp. 35–51.
13. P. J. Brenchley *et al.*, *Geology* **22**, 295 (1994).
14. B. D. Webby, F. Paris, M. L. Droser, I. G. Percival, *The Great Ordovician Biodiversification Event* (Columbia Univ. Press, New York, 2004).
15. J. J. Sepkoski, in *Ordovician Odyssey: Short papers for the Seventh International Symposium on the Ordovician System*, J. D. Cooper, M. L. Droser, S. C. Finney, Eds. (The Pacific Section Society for Sedimentary Geology, Fullerton, 1995), pp. 393–396.
16. M. M. Joachimski, W. Buggisch, *Geology* **30**, 711 (2002).
17. M. M. Joachimski, R. van Geldern, S. Breisig, W. Buggisch, J. Day, *Int. J. Earth Sci.* **93**, 542 (2004).
18. B. Wenzel, C. Lйcuyer, M. M. Joachimski. *Geochim. Cosmochim. Acta* **64**, 1859 (2000).
19. Values were normalized to National Bureau of Standards (NBS) 120c values of 22.4‰. Our $\delta^{18}O$ values were normalized to 21.7‰. These values will affect the calculated temperatures.
20. M. M. Joachimski, P. H. von Bitter, W. Buggisch, *Geology* **34**, 277 (2006).
21. Assuming $\delta^{18}O_{seawater} = -1$ for an ice-free world that would be consistent with modern values.
22. Materials, methods, and data tables are available as supporting material on *Science* Online.
23. L. R. M. Cocks, T. H. Torsvik, in *The Great Ordovician Biodiversification Event*, B. D. Webby, F. Paris, M. L. Droser, I. G. Percival, Eds. (Columbia Univ. Press, New York, 2004), pp. 61–67.
24. D. Bassett, K. G. Macleod, J. F. Miller, R. L. Ethington, *Palaios* **22**, 98 (2007).
25. The ~1‰ shift includes an unconstrained ice volume contribution so the temperature component would be less than 5°C.
26. E. G. Kauffman, J. A. Fagerstrom, in *Species Diversity in Ecological Communities: Historical and Geographical Perspectives*, R. E. Ricklefs, D. Schluter, Eds. (Univ. of Chicago Press, Chicago, 1993), pp. 315–329.
27. J. Veizer, Y. Godderis, L. M. François, *Nature* **408**, 698 (2000).
28. R. E. Came *et al.*, *Nature* **449**, 198 (2007).
29. N. J. Shaviv, J. Veizer, *GSA Today* **13**, 4 (2003).
30. X. Chen, Y.-D. Zhang, J. X. Fan, *Geol. J.* **41**, 289 (2006).
31. P. J. Noble, T. Danelian, in *The Great Ordovician Biodiversification Event*, B. D. Webby, F. Paris, M. L. Droser, I. G. Percival, Eds. (Columbia Univ. Press, New York, 2004), pp. 97–101.
32. K. J. Peterson, *Geology* **33**, 929 (2005).
33. R. A. Berner, *Geochim. Cosmochim. Acta* **70**, 5653 (2006).
34. B. Schmitz *et al.*, *Nat. Geosci.* **1**, 49 (2008).
35. P. J. Brenchley, in *The Great Ordovician Biodiversification Event*, B. D. Webby, F. Paris, M. L. Droser, I. G. Percival, Eds. (Columbia Univ. Press, New York, 2004), pp. 81–83.
36. C. Lécuyer *et al.*, *Geochim. Cosmochim. Acta* **62**, 2429 (1998).
37. The "ice volume" contribution to $\delta^{18}O$ is also a function of its isotopic composition, which today varies between −40 and -25‰.
38. M. R. Saltzman, S. A. Young, *Geology* **33**, 109 (2005).

39. The development of SHRIMP in situ oxygen isotope analysis was partly funded by the Australian Research Council (grant DP0559604 to I.S.W.). An Australian Postgraduate Award financed J.A.T.'s Ph.D. conodont geochemistry research, and the Paleontological Society and Mid-American Paleontological Society awarded a student bursary to J.A.T. P. Holden, R. Ickert, and J. Hiess contributed to developing the oxygen isotope analytical procedures. M. McCulloch and B. Webby provided comments that improved the manuscript.

Supporting Online Material

www.sciencemag.org/cgi/content/full/321/5888/550/DC1
Materials and Methods
Fig. S1
Tables S1 and S2
References

29 January 2008; accepted 17 June 2008
10.1126/science.1155814

Enhancement of Thermoelectric Efficiency in PbTe by Distortion of the Electronic Density of States

Joseph P. Heremans,[1,2]* Vladimir Jovovic,[1] Eric S. Toberer,[3] Ali Saramat,[3] Ken Kurosaki,[4] Anek Charoenphakdee,[4] Shinsuke Yamanaka,[4] G. Jeffrey Snyder[3]*

The efficiency of thermoelectric energy converters is limited by the material thermoelectric figure of merit (zT). The recent advances in zT based on nanostructures limiting the phonon heat conduction is nearing a fundamental limit: The thermal conductivity cannot be reduced below the amorphous limit. We explored enhancing the Seebeck coefficient through a distortion of the electronic density of states and report a successful implementation through the use of the thallium impurity levels in lead telluride (PbTe). Such band structure engineering results in a doubling of zT in p-type PbTe to above 1.5 at 773 kelvin. Use of this new physical principle in conjunction with nanostructuring to lower the thermal conductivity could further enhance zT and enable more widespread use of thermoelectric systems.

Thermoelectric (TE) energy conversion is an all-solid-state technology used in heat pumps and electrical power generators. In essence, TE coolers and generators are heat engines thermodynamically similar to conventional vapor power generation or heat pumping cycles, but they use electrons as the working fluid instead of physical gases or liquids. Thus, TE coolers and generators have no moving fluids or moving parts and have the inherent advantages of reliability, silent and vibration-free operation, a very high power density, and the ability to maintain their efficiency in small-scale applications where only a moderate amount of power is needed. In addition, TE power generators directly convert temperature gradients and heat into electrical voltages and power, without the additional need for an electromechanical generator.

All of these properties make them particularly suited for recovering electrical power from otherwise wasted heat, for instance in automotive exhaust systems or solar energy converters. These advantages are partially offset by the relatively low efficiency of commercially available material, limiting the use of the technology to niche applications for the past half century. Recent efforts have focused on nanostructured materials to enhance the TE efficiency.

The efficiency of thermoelectric generators is limited to a fraction of their Carnot efficiency ($\eta_c = \Delta T/T_H$), determined by the dimensionless thermoelectric material figure of merit (*1*), zT:

$$zT = T\frac{S^2\sigma}{\kappa} \qquad (1)$$

where S is the thermoelectric power or Seebeck coefficient of the TE material, σ and κ are the electrical and thermal conductivities, respectively, and T is the absolute temperature. For the past four decades, zT of commercial material has been limited to about 1 in all temperature ranges (*1*).

[1]Department of Mechanical Engineering, Ohio State University, 201 West 19th Avenue, Columbus, OH 43210, USA. [2]Department of Physics, Ohio State University, 201 West 19th Avenue, Columbus, OH 43210, USA. [3]California Institute of Technology, Pasadena, CA 91125, USA. [4]Graduate School of Engineering, Osaka University, Suita, Osaka 565-0871, Japan.

*To whom correspondence should be addressed. E-mail: heremans.1@osu.edu (J.P.H.); jsnyder@caltech.edu (G.J.S.)

Recent progress in TE materials has primarily involved decreasing the denominator of Eq. 1 by creating materials with nanometer-scaled morphology to dramatically lower the thermal conductivity by scattering phonons. Quantum-dot superlattices have reported values of $zT > 2$ (*2*), and silicon nanowires have such a reduced κ that zT approaches that of commercial materials (*3*). Although this certainly provides the evidence that high-zT material can be prepared, the results were obtained on thin films or nanowires that are challenging for high-volume applications that normally rely on bulk materials. Structural complexity on various length scales has successfully reduced κ in bulk TE materials, also yielding $zT > 1$ (*1*, *4*–*8*).

Unfortunately, in bulk material at least, there is a lower limit to the lattice thermal conductivity imposed by wave mechanics: The phonon mean free path cannot become shorter than the interatomic distance (*9*). The minimum thermal conductivity of PbTe is about 0.35 W/mK at 300 K, a value measured on quantum-dot superlattices (*2*). Although lower values have been seen for interfacial heat transfer (*10*), progress beyond this point in bulk materials must come from the numerator of Eq. 1 and in particular the Seebeck coefficient; we describe here a successful approach in this direction for bulk materials.

A strong increase has been predicted in the Seebeck coefficient of nanostructures (*11*, *12*) and was observed experimentally in Bi nanowires (*13*). The basis for the enhancement of S here is the Mahan-Sofo theory (*14*), which suggests the study of systems in which there is a local increase in the density of states (DOS) $g(E)$ over a narrow energy range (E_R), as shown schematically in Fig. 1A. Such a situation can occur when the valence or conduction band of the host semiconductor resonates with one energy level of a localized atom in a semiconductor matrix (*14*). The effect of this local increase in DOS on S is given by the Mott expression (Eq. 2). Here, S depends on the energy derivative of the energy-dependent electrical conductivity $\sigma(E) = n(E)q\mu(E)$ taken at the Fermi energy E_F (*15*), with $n(E) = g(E)f(E)$, the carrier density at the energy level E considered, where $f(E)$ is the Fermi function, q the carrier charge, and $\mu(E)$ the mobility:

$$S = \frac{\pi^2}{3}\frac{k_B}{q}k_B T\left\{\frac{d[\ln(\sigma(E))]}{dE}\right\}_{E=E_F} = \frac{\pi^2}{3}\frac{k_B}{q}k_B T\left\{\frac{1}{n}\frac{dn(E)}{dE} + \frac{1}{\mu}\frac{d\mu(E)}{dE}\right\}_{E=E_F} \quad (2)$$

Equation (2) shows that there are two mechanisms that can increase S: (i) an increased energy-dependence of $\mu(E)$, for instance by a scattering mechanism that strongly depends on the energy of the charge carriers, or (ii) an increased energy-dependence of $n(E)$, for instance by a local increase in $g(E)$. Mechanism (ii) is the basis of the Mahan-Sofo theory, provided that E_F of the semiconductor aligns properly in the range of the excess DOS in the band (Fig. 1A). The concept can also be expressed in terms of effective mass m^*_d, as shown for degenerate semiconductors (*1*):

$$S = \frac{8\pi^2 k_B^2 T}{3qh^2} m_d^* \left(\frac{\pi}{3n}\right)^{2/3} \quad (3)$$

with

$$g(E) = \frac{(m_d^*)^{3/2}\sqrt{2E}}{\hbar^3 \pi^2} \quad (4)$$

Because zT also depends on the carrier's group velocity via the electrical conductivity, the value of E_F that maximizes zT is somewhat different from the value that maximizes S and m^*_d (*14*).

Calculations (*16*) indicate that the group III elements Ga, In, and Tl create additional energy levels, sometimes called resonant levels, in a classical thermoelectric semiconductor, PbTe. We report here that the approach is successful in doubling zT in dilute alloys of PbTe with 1 or 2 atomic % Tl (Tl-PbTe) (Fig. 1B). Review articles have described how the group III elements establish states in the IV-VI compound semiconductors (*17*, *18*). The origin of the Tl-induced states is still under investigation, and they have been ascribed to either a valence fluctuation (*18*) or a hybridization between an excited state of the group III atom and the neighboring Te p-states (*16*), or an additional piece of the Fermi surface (*19*). Considering now all group III atoms in PbTe, we see that the position of the additional energy level is not clear in Ga-PbTe (*17*, *18*), that for In-PbTe it is favorably located in the conduction band at low temperature (*20*) but moves into the energy gap at room temperature (*21*), and that it is favorably located in the valence band of Tl-PbTe (*17*).

Optical measurements suggest that there are several distinct levels associated with Tl in PbTe, one of which is at an energy ~ 0.06 eV below the band edge; the width of such levels depends on the exact composition of the alloy but is on the order of ~0.03 eV (*17*). The strong influence of the Tl level on the valence band of Tl-PbTe is further confirmed by measurements of the electronic specific heat (*22*), which show an increase in the density of available electronic states in the valence band over that of pure PbTe as a function of Tl concentration. An increase by a factor of 2.6 is observed at 1.5 atomic % Tl. The increase is also related to the surprisingly high superconductive transition temperature in the material.

Several disk-shaped samples of $Tl_{0.01}Pb_{0.99}Te$ and $Tl_{0.02}Pb_{0.98}Te$ were prepared (*23*) and mounted for high-temperature measurements (300 to 773 K) of their conductivity (σ and κ), as well as Hall (R_H) and Seebeck (S) coefficients; parallelepipedic samples were cut from the disks and mounted for low-temperature measurements (77 K to 400 K) of galvanomagnetic (ρ and R_H) and thermomagnetic (S and N, which stands for the isothermal transverse Nernst-Ettingshausen coefficient) properties (*23*). The results for the zero-field transport properties measured on representative samples of $Tl_{0.01}Pb_{0.99}Te$ and $Tl_{0.02}Pb_{0.98}Te$ are shown in Fig. 2.

Values of zT for $Tl_{0.02}Pb_{0.98}Te$ reach 1.5 at 773 K (Fig. 1B). The high value of zT observed is quite reproducible and robust with respect to slight variation in dopant concentration in $Tl_{0.02}Pb_{0.98}Te$. The uncertainty in zT is estimated to be on the order of 7% near room temperature and increasing at higher temperature if we assume that the inaccuracies on S, σ and κ are independent of each other (*23*). For the $Tl_{0.01}Pb_{0.99}Te$, the decreased doping levels lead to a lower carrier concentration and a corresponding increase in S and ρ. The values in Fig. 1B represent a 100% improvement of the zT compared with the best conventional p-type PbTe-based alloys ($zT_{max} = 0.71$ for $Na_{0.01}Pb_{0.99}Te$) (*24*). The maximum in zT occurs at the temperature where thermal excitations start creating minority carriers. This maximum is not reached by 773 K for $Tl_{0.02}Pb_{0.98}Te$, and thus, higher values of zT may be expected.

The temperature range where these PbTe-based materials exhibit high zT values (500 to 773 K) is appealing for power generation from waste heat sources such as automobile exhaust.

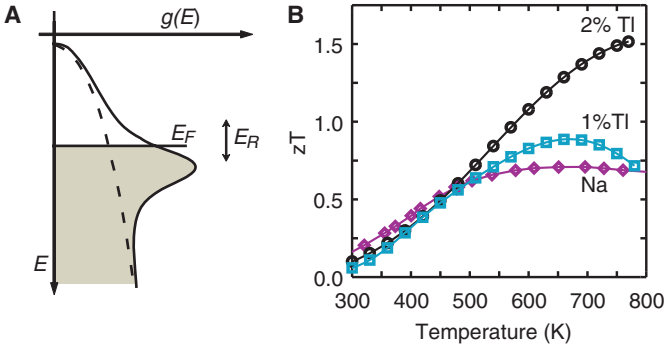

Fig. 1. (**A**) Schematic representation of the density of electron states of the valence band of pure PbTe (dashed line) contrasted to that of Tl-PbTe in which a Tl-related level increases the density of states. The figure of merit zT is optimized when the Fermi energy E_F of the holes in the band falls in the energy range E_R of the distortion. (**B**) The zT values for $Tl_{0.02}Pb_{0.98}Te$ (black squares) and $Tl_{0.01}Pb_{0.99}Te$ (blue circles) compared to that of a reference sample of Na-PbTe (purple diamonds).

Direct thermoelectric efficiency measurements were not conducted because of the nontrivial requirements for a matching *n*-type material, good thermal isolation, and low thermal and electrical contact resistance. The latter consideration arises because the main flow of heat and of electrical current must pass through the contacts of a TE power generator, in contrast to the situation in the experiments reported here.

The κ values of every Tl-PbTe sample measured reproduces that of pure bulk PbTe (*25*). In contrast, all *zT* -enhancing mechanisms used previously in PbTe-based materials have relied on minimizing the lattice thermal conductivity (*1*, *4*, *7*, *8*). The slight rise in κ of the $Tl_{0.02}Pb_{0.98}Te$ sample at high temperatures is attributed to ambipolar thermal conduction.

We analyzed Hall and Nernst coefficients (*23*) to elucidate the physical origin of the enhancement in *zT*. The Hall coefficient R_H of $Tl_{0.02}Pb_{0.98}Te$ is nearly temperature independent up to 500 K, corresponding to a hole density of 5.3×10^{19} cm^{-3}. The room temperature hole mobility μ ($\mu = R_H/\rho$) for $Tl_{0.02}Pb_{0.98}Te$ varies from sample to sample between 50 and 80 cm^2/Vs and is a factor of 5 to 3 smaller than the mobility of single-crystal PbTe at similar carrier concentrations (*26*) but has a similar temperature dependence.

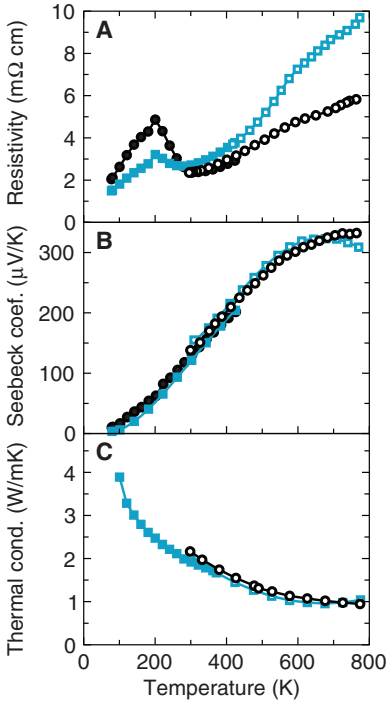

Fig. 2. Temperature dependence of the (**A**) resistivity, (**B**) Seebeck coefficient, and (**C**) thermal conductivity of a representative sample of $Tl_{0.02}Pb_{0.98}Te$ and of $Tl_{0.01}Pb_{0.99}Te$, using the same conventions as in Fig. 1. The open and closed symbols represent data taken in two different measurement systems.

As seen in Eq. 3, typically *S* depends strongly on carrier density. The solid line, known as a Pisarenko plot (*27*), shown in Fig. 3, was calculated given the known band structure and acoustic phonon scattering; almost every measurement published on *n* or *p*-type bulk PbTe falls on that line (*25*). Compared to this, *S* of Tl-PbTe at 300 K is enhanced at the same carrier concentration, as shown graphically in Fig. 3, where we show data on every Tl-PbTe sample measured in this study. All show an enhancement in *S* by a factor of between 1.7 and 3, which, in $Tl_{0.02}Pb_{0.98}Te$ samples, more than compensates for the loss in mobility in *zT*. The enhancement increases with carrier density, and indeed so does the *zT*.

We recall from Eq. 2 that *S* is a function of the energy dependence of both the density of states and the mobility. The mobility can be represented in terms of a relaxation time τ and a transport effective mass m^*: $\mu = q\tau/m^*$. The energy dependence of the relaxation time ($\tau(E) = \tau_0 E^{\Lambda}$) (*25*) is taken to be a power law, with the power, the scattering exponent Λ, determined by the dominant electron scattering mechanism. Acoustic phonon scattering in a three-dimensional solid is characterized by $\Lambda = -1/2$.

Nernst coefficient measurements (*23*) make it possible to determine the scattering exponent Λ and to decide which of the two terms in Eq. 2 dominates. We use the "method of the four coefficients" (*28*), developed to deduce μ, Λ, m^*_d and E_F from measurements of ρ, R_H, *S*, and *N*. We observe no increase in Λ over its value (−1/2) in pure PbTe (*28*) as would be expected from the "resonant scattering" (*29*) hypothesis. Furthermore, the effects of resonant scattering (*29*) would be expected to vanish with increasing temperature, because acoustic and optical phonon scattering would then become ever more dominating. This would not only contradict the results of Fig. 1 but also preclude the use of the mechanism in any high-temperature applications such as electrical power generators.

In contrast to the constant scattering exponent Λ, the method of four coefficients shows a factor of 3 increase in the effective mass (m_d^*) over that of Na-PbTe (Fig. 4) (*30*) calculated at E_F = 50 meV for a classical nonparabolic band (*25*). As seen in Eq. 3, such an increase in m_d^* will directly increase *S* by the same factor, as observed. It is also consistent with the measurements of the electronic specific heat (*22*), as expected because both the specific heat and *S* are closely related to the entropy of the electrons (*31*). The local increase in m_d^* implies a decidedly nonparabolic perturbation in the electron dispersion relations and the density of states.

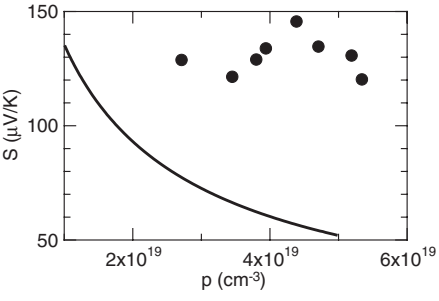

Fig. 3. Pisarenko relation of Seebeck coefficient at 300 K versus hole concentration for PbTe (solid line) compared to the results measured on every Tl-PbTe sample prepared for this study.

Because *S* and electronic heat capacity are sensitive to the change in the DOS at E_F, m_d^* derived from these quantities is actually a measure of *dn*(E)/*d*E. The latter quantity will be enhanced for E_F close to the inflection point of the *g(E)* curve (Fig. 1A), which is closer to the valence band edge than the energy at which the DOS is maximum; Indeed, there need not even be a maximum in *g(E)* for the argument to hold. The measured value of E_F at 50 meV is consistent with this description, because the inflection point is expected to be near half the energy (~30 meV in this case) at which a maximum in DOS is reported (*17*). In general, the sharper the local increase in DOS, the larger the enhancement in m_d^* and in *S*. The agreement between the measurements of the enhancement in m_d^*, specific heat, and our measured E_F for Tl-PbTe strongly supports this model as the source of enhanced *S* and *zT*.

One signature feature we observed in every Tl-PbTe sample measured is the local maximum in ρ near 200 K. It is attributed to a minimum in mobility that occurs at the same temperature at which the mass has a maximum. Thus, we suggest that the maximum in ρ, or the minimum in μ, occur at a temperature at which E_F nears an inflection point in the dispersion relation, although a much more detailed analysis involving the study of double-doped samples with variable E_Fs is necessary to reach firm conclusions.

Further improvements in *zT* should be possible by systematically searching for the optimum location of E_F compared to the shape of *g(E)*, for instance, by co-doping the samples with both Tl and another acceptor impurity such as Na. In addition to opening a new route to high-*zT* materials that is not limited by the concept of minimum κ, this approach does not rely on the

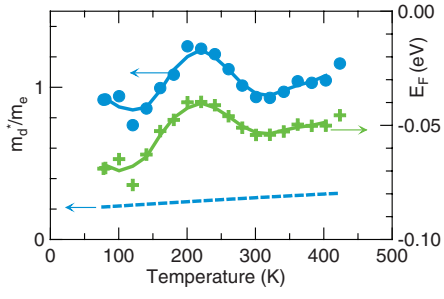

Fig. 4. Temperature dependence of the Fermi energy (green + symbols, right ordinate, the zero referring to the top of the valence band) and of the density of states effective mass (blue dots, left ordinate) of $Tl_{0.02}Pb_{0.98}Te$ compared to that of Na-PbTe (blue dashed line).

formation of nanoparticles, which are subject to grain growth or dissolution into the host material during operation. The method is independent of phonon properties, implying that improvements in zT induced by reducing the lattice κ value can work in conjunction with the mechanism described here. We anticipate that deliberately engineered impurity-induced band-structure distortions will be a generally applicable route to enhanced S and zT in all TE materials. We are optimistic about the commercial use of such PbTe-based materials because there is an extensive knowledge base among the manufacturers of thermoelectric generators about the assembly of PbTe-based devices, in particular the ability to make stable metallic contacts with low thermal and electrical resistance.

References and Notes

1. G. J. Snyder, E. S. Toberer, *Nat. Mater.* **7**, 105 (2008).
2. T. C. Harman *et al.*, *Science* **297**, 2229 (2002).
3. A. I. Hochbaum *et al.*, *Nature* **451**, 163 (2008).
4. K. F. Hsu *et al.*, *Science* **303**, 818 (2004).
5. B. Poudel *et al.*, *Science* **320**, 634 (2008)
6. B. Sales *et al.*, *Science* **5266**, 1325 (1998).
7. J. Androulakis *et al.*, *Adv. Mater.* **18**, 1170 (2006).
8. P. F. R. Poudeu *et al.*, *Angew. Chem. Int. Ed.* **45**, 3835 (2006).
9. G. A. Slack, in *Solid State Physics, Vol. 34*, H. Ehrenreich, F. Seitz, D. Turnbull, Eds. (Academic Press, New York, 1979), pp. 1–71.
10. R. H. Costescu *et al.*, *Science* **303**, 989 (2004).
11. L. D. Hicks, M. S. Dresselhaus, *Phys. Rev. B* **47**, 12727 (1993).
12. L. D. Hicks, M. S. Dresselhaus, *Phys. Rev. B* **47**, 16631 (1993).
13. J. P. Heremans *et al.*, *Phys. Rev. Lett.* **88**, 216801 (2002).
14. G. D. Mahan, J. O. Sofo, *Proc. Natl. Acad. Sci. U.S.A.* **93**, 7436 (1996).
15. M. Cutler, N. F. Mott, *Phys. Rev.* **181**, 1336 (1969).
16. S. Ahmad *et al.*, *Phys. Rev. Lett.* **96**, 056403 (2006).
17. S. A. Nemov *et al.*, *Physics-Uspekhi* **41**, 735 (1998).
18. B. A. Volkov *et al.*, *Physics-Uspekhi* **45**, 819 (2002).
19. K. Nakayama *et al.*, *Phys. Rev. Lett.* **100**, 227004 (2008).
20. V. Jovovic *et al.*, *J. Appl. Phys.* **103**, 053710 (2008).
21. V. Jovovic *et al.*, in *Mater. Res. Soc. Symp. Proc.* 1044, T. P. Hogan, J. Yang, R. Funahashi, T. Tritt, Eds. (Materials Research Society, Warrendale, PA, 2008), U04-09.
22. Y. Matsushita *et al.*, *Phys. Rev. B* **74**, 134512 (2006).
23. Materials and methods are available as supporting material on *Science* Online.
24. R. W. Fritts, in *Thermoelectric Materials and Devices*, I. B. Cadoff, E. Miller, Eds. (Reinhold, New York, 1960), pp. 143–162.
25. Yu. I. Ravich *et al.*, *Semiconducting Lead Chalcogenides* (Plenum, New York, 1970).
26. We have not been able to find the carrier-density dependence of the hole mobility for PbTe. For electrons, at 300 K, $\mu_e \approx 550$ cm^2/Vsat, $n = 5 \times 10^{19}$ cm^{-3} (*32*), whereas the ratio of electron to hole mobility at $n \approx 3 \times 10^{18}$ cm^{-3} and 300 K is 2.2 (*33*), so that we estimate the hole mobility to be about 250 cm^2/Vs 5×10^{19} cm^{-3}.
27. A. F. Ioffe, *Semiconductor Thermoelements and Thermoelectric Cooling*, (Infosearch Limited, London, 1957).
28. J. P. Heremans *et al.*, *Phys. Rev. B* **70**, 115334 (2004).
29. Ravich (*34*) suggests that the energy dependence of the hole scattering on the resonant states (resonant scattering) increases S by increasing the second term, $d\mu/dE$, and therefore the low temperature zT.
30. H. Preier, *Appl. Phys. (Berl.)* **20**, 189 (1979).
31. H. B. Callen, *Thermodynamics* (Wiley, New York, 1960).
32. Yu. I. Ravich *et al.*, *Phys. Status Solidi B* **43**, 453 (1971).
33. R. S. Allgaier, W. W. Scanlon, *Phys. Rev.* **111**, 1029 (1958).
34. Yu. I. Ravich, in *CRC Handbook of Thermoelectrics*, D. M. Rowe, Ed. (CRC Press, Boca Raton, FL, 1995), pp. 67–81.

35. This work was supported by the BSST Corporation, the State of Ohio Department of Development's Center for Photovoltaic Innovation of Commercialization (OSU), the Beckman Institute, the Swedish Bengt Lundqvist Minne Foundation, and Jet Propulsion Laboratory, NASA (Caltech). Patent protection related to this work is pending.

Supporting Online Material

www.sciencemag.org/cgi/content/full/321/5888/554/DC1
Materials and Methods
Fig. S1
References

28 April 2008; accepted 17 June 2008
10.1126/science.1159725

BSKs Mediate Signal Transduction from the Receptor Kinase BRI1 in *Arabidopsis*

Wenqiang Tang,[1] Tae-Wuk Kim,[1] Juan A. Oses-Prieto,[2] Yu Sun,[1] Zhiping Deng,[1] Shengwei Zhu,[1,3] Ruiju Wang,[1,4] Alma L. Burlingame,[2] Zhi-Yong Wang[1]*

Brassinosteroids (BRs) bind to the extracellular domain of the receptor kinase BRI1 to activate a signal transduction cascade that regulates nuclear gene expression and plant development. Many components of the BR signaling pathway have been identified and studied in detail. However, the substrate of BRI1 kinase that transduces the signal to downstream components remains unknown. Proteomic studies of plasma membrane proteins lead to the identification of three homologous BR-signaling kinases (BSK1, BSK2, and BSK3). The BSKs are phosphorylated by BRI1 in vitro and interact with BRI1 in vivo. Genetic and transgenic studies demonstrate that the BSKs represent a small family of kinases that activate BR signaling downstream of BRI1. These results demonstrate that BSKs are the substrates of BRI1 kinase that activate downstream BR signal transduction.

Cell-surface receptor kinases activate cellular signal transduction pathways upon perception of extracellular signals, thereby mediating cellular responses to the environment and to other cells. The *Arabidopsis* genome encodes more than 400 receptor-like kinases (RLKs) (*1*). Some of these RLKs function in growth regulation and plant responses to hormonal and environmental signals. However, the molecular mechanism of RLK signaling to immediate downstream components remains poorly understood, as no RLK substrate that mediates signal transduction has been established in *Arabidopsis* (*2*). BRI1 is an RLK that functions as the major receptor for the steroid hormones brassinosteroids (BRs) (*2*). BRs bind the extracellular domain of BRI1 to activate its kinase activity, initiating a signal transduction cascade that regulates nuclear gene expression and a wide range of developmental and physiological processes (fig. S1) (*3*). Many components of the BR signaling pathway have been identified, and much detail has been revealed about how BR activates BRI1 (*4*–*8*) and how phosphorylation by downstream GSK3-like kinase BIN2 regulates the activity of the nuclear transcription factors that mediate BR-responsive gene expression (fig. S1) (*3*, *9*–*13*). However, no direct interaction has been observed between BRI1 and BIN2, and it remains unclear how BRI1 kinase at the plasma membrane transduces the signal to cytoplasmic components of the BR pathway (*14*).

To identify additional components of the BR signaling pathway, we performed quantitative proteomic studies of BR-responsive proteins using two-dimensional difference gel electrophoresis (2D DIGE). Seedlings of BR-deficient *det2-1* mutant were treated with brassinolide (BL) (the most active form of BRs) or mock solution, and proteins were labeled with Cy3 or Cy5 dyes, mixed together, and separated in the same gel by 2D gel electrophoresis (2-DE). BL-induced BAK1 phosphorylation and BZR1 dephosphorylation were detected in the plasma membrane and phosphoprotein fractions, respectively (*15*), but not in total proteins (*16*). Similar to BAK1, two additional rows of spots showed a BR-induced increase of the acidic forms and a decrease of the basic forms (Fig. 1, A and B), which is consistent with BR-induced phosphorylation. Mass spectrometry analysis of these spots identified two kinases encoded by *Arabidopsis* genes At4g35230 and At5g46570, which we named BR-signaling kinases 1 and 2 (BSK1 and BSK2) (Fig. 1B and

[1]Department of Plant Biology, Carnegie Institution of Washington, Stanford, CA 94305, USA. [2]Department of Pharmaceutical Chemistry, University of California, San Francisco, CA 94143, USA. [3]Key Laboratory of Photosynthesis and Environmental Molecular Biology, Institute of Botany, Chinese Academy of Sciences, Beijing 100093, China. [4]Institute for Molecular Biology, College of Life Science, Nankai University, Tianjin 300071, China.

*To whom correspondence should be addressed. E-mail: zywang24@stanford.edu